Fluid Dynamics &
Materials Processing

Tech Science Press

http://doi.org/10.32604/fdmp.2026.080521

ARTICLE

Optimizing Groove-Enhanced Microchannels for High-Performance Heat Dissipation

Hongxin Zhang*,#, Yi Zhang#, Jiyun Tang* and Lei Yao

School of Energy and Control Engineering, Changji University, Changji, China
*Corresponding Authors: Hongxin Zhang. Email: zhx_xj@sina.com; Jiyun Tang. Email: jiyun_tang@163.com
#These authors contributed equally to this paper and are both listed as first authors

Received: 11 February 2026; Accepted: 21 April 2026; Published: 07 May 2026

ABSTRACT: Traditional parallel straight microchannels are limited by low heat flux density and non-uniform flow distribution. From a system optimization perspective, incorporating surface grooves provides an effective means to enhance solid-liquid interaction and improve overall performance. Using water as the working fluid, this study numerically investigates the coupled effects of inlet flow rate, groove number, and groove spacing on the thermo-hydraulic behavior of groove-type microchannel heat sinks. The results reveal a fundamental trade-off between heat transfer enhancement and hydraulic resistance. Increasing coolant velocity significantly improves heat dissipation, but also raises the pressure drop, affecting pumping power and system stability. Likewise, grooves act as flow-disturbing elements that induce separation and vortex formation, thereby enhancing convective heat transfer while increasing flow resistance. For fixed channel length and groove number, optimizing groove spacing enables a balanced improvement in heat transfer and reduction in pressure losses. Overall, the findings frame the design as a multi-objective optimization problem, where thermal performance, pressure drop, and energy efficiency must be simultaneously considered. It is shown that proper selection of groove configuration ensures efficient heat removal, stable fluid circulation, accurate temperature control, and minimized energy consumption due to excessive pressure losses.

KEYWORDS: Groove; flow disturber; microchannel; simulation; thermal dissipation characteristics

1 Introduction

With the miniaturization, modularization, and increased power density of electronic components, their heat flux density has surged dramatically [1,2]. The resulting thermal management and heat distribution challenges have become major obstacles, affecting the stability of electronic systems and limiting the performance development of electronic devices [3,4]. Taking microelectronic chips as an example, the heat flux density generated by chips typically ranges from 60 to 90 W/cm^2, with peak values as high as 200 W/cm^2 [5,6]. Efficient heat dissipation is a critical factor affecting the stable operation of components. Such high heat flux density can cause localized temperature spikes in high-heat-generating components within confined spaces, thereby significantly impacting the performance of electronic components and equipment. Implementing efficient, rapid heat dissipation for high-heat-flux-density electronic components through rational thermal management methods, thereby maintaining their operating temperatures within stable working ranges, has become a critical technology for enhancing the reliability of electronic components [7]. Consequently, thermal management systems at the micro-scale are indispensable [8].

Microchannel heat transfer, as a heat transfer device with a high surface-to-volume ratio, exhibits exceptionally high heat transfer performance [9,10]. Compared to conventional-sized channels, microchannels feature significantly smaller structural dimensions. The thickness of the fluid boundary layer is significantly reduced due to the constraints of the narrow microchannel structure, resulting in a decrease in flow thermal resistance, which in turn effectively enhances heat transfer efficiency and improves overall heat transfer performance. This micro-scale thermal system features compact size, low energy consumption, and cost-effectiveness, offering immense application potential in fields such as communications, microelectronics, automotive, medical technology, laser technology, and aerospace.

The concept of micro-scale array channels was first put forward by Tuckerman and Pease [11], who successfully removed heat at a heat flux density of 1000 W/cm^2. However, as the thermal load on microelectronic devices continues to increase, smooth-walled microchannels are no longer suitable. Therefore, it is necessary to further optimize and improve the heat transfer characteristics of microchannels in order to enhance their overall heat transfer capacity. Among these, increasing the solid-liquid contact surface area is a highly effective method. For instance, incorporating recesses and internal ribs, such complex microchannel structures can effectively meet the growing thermal management demands of modern miniature electronic devices.

Now, studies on groove-type microchannel radiators have focused on structural optimization, heat transfer mechanisms, and performance trade-offs. The relevant researchers have systematically explored the effects of groove geometry (shape, aspect ratio, pitch) on heat transfer and flow resistance. For instance, Zhu et al. [12] found triangular grooves achieve optimal heat transfer enhancement while teardrop grooves balance thermal-hydraulic performance. Kumar et al. [13] demonstrated trapezoidal grooves improve heat transfer efficiency by 12% compared to rectangular counterparts.

Research has also been conducted focusing on practical electronic cooling applications. For instance, Liu et al. [14] optimized fan-shaped reentrant grooves, finding a pitch-width ratio of 3 maximizes heat transfer while minimizing pressure drop. Lv et al. [15] confirmed rectangular groove walls enhance critical heat flux (CHF) by 31.3% through improved liquid film wetting. Composite designs integrating grooves with ribs or cavities have gained attention, as Wang et al. [16] reported fan-shaped grooves combined with triangular ribs yield a Nusselt number of 1.081. Machine learning and multi-objective optimization are increasingly used to address the heat transfer-resistance trade-off [17].

Extensive research has been conducted on microchannel heat sinks (MCHSs) with cavity or grooved/ribbed structures to enhance thermal performance. Kuo and Peles [18] fabricated multiple sets of recessed cavity structures in a silica microchannel; these structural units are separated from one another but exhibit local connectivity. Sitar et al. [19] designed triangular, conical, circular, and sharp-edged etched recesses, respectively, to improve boiling heat transfer characteristics through the use of irregular cavity structures. Subsequent numerical studies further quantified the effects of cavity geometry: Xia et al. [20] optimized triangular cavity MCHSs by adjusting cavity distance and shape, and Hou and Chen [21] demonstrated that circular cavities outperformed trapezoidal and rectangular counterparts. Liu et al. [22] extended this to a double-layer interleaved cavity MCHS, which exhibited superior thermal-hydraulic performance compared to both straight channels and single-layer triangular cavity designs.

Despite these advances, the existing literature is primarily limited to discrete cavity structures or conventional grooved/ribbed microchannels, and there are still shortcomings in simulating microscale effects and optimizing complex grooves under extreme heat flux conditions; in particular, further research is needed regarding groove spacing and the number of grooves. Further integration of experimental validation and advanced numerical models is required [23]. Therefore, this paper employs numerical calculation

methods to investigate the influence patterns of working fluid velocity, groove quantity, and groove spacing on the heat dissipation characteristics of microchannel heat sinks.

The main structure of this paper is as follows: Section 2 introduces the numerical simulation, including the governing equations, physical models, mesh generation, and boundary conditions; Section 3 presents the results and discussion, focusing on the effects of working fluid velocity, groove number, and groove spacing on the heat dissipation performance of groove-type microchannel heat exchangers; Section 4 concludes the study.

2 Numerical Simulation

2.1 Control Equation

The fluid domain medium studied in this paper is an incompressible Newtonian fluid, encompassing the fundamental principles of mass conservation and momentum conservation, which can be expressed as:

Law of conservation of mass:

$$\frac{\partial u}{\partial x}+\frac{\partial v}{\partial y}+\frac{\partial w}{\partial z}=0, \tag{1}$$

here, u, v, and w denote the velocity components along the x, y, and z coordinate axes, respectively.

Momentum conservation equations:

The momentum equations along the X, Y, and Z directions are as follows:

X-axis:

$$\rho\left(\frac{\partial u}{\partial t}+u\frac{\partial u}{\partial x}+v\frac{\partial u}{\partial y}+w\frac{\partial u}{\partial z}\right)=-\frac{\partial p}{\partial x}+\mu\left(\frac{\partial^2 u}{\partial x^2}+\frac{\partial^2 u}{\partial y^2}+\frac{\partial^2 u}{\partial z^2}\right) \tag{2}$$

Y-axis:

$$\rho\left(\frac{\partial v}{\partial t}+u\frac{\partial v}{\partial x}+v\frac{\partial v}{\partial y}+w\frac{\partial v}{\partial z}\right)=-\frac{\partial p}{\partial y}+\mu\left(\frac{\partial^2 v}{\partial x^2}+\frac{\partial^2 v}{\partial y^2}+\frac{\partial^2 v}{\partial z^2}\right) \tag{3}$$

Z-axis:

$$\rho\left(\frac{\partial w}{\partial t}+u\frac{\partial w}{\partial x}+v\frac{\partial w}{\partial y}+w\frac{\partial w}{\partial z}\right)=-\frac{\partial p}{\partial z}+\mu\left(\frac{\partial^2 w}{\partial x^2}+\frac{\partial^2 w}{\partial y^2}+\frac{\partial^2 w}{\partial z^2}\right) \tag{4}$$

where ρ, μ, and p correspond to the working fluid density, dynamic viscosity, and pressure, respectively, and t denotes time.

Energy conservation equation:

For the steady-state, incompressible flow with negligible viscous dissipation and internal heat sources, the energy conservation equation is expressed as:

$$\rho c_p\left(u\frac{\partial T}{\partial x}+v\frac{\partial T}{\partial y}+w\frac{\partial T}{\partial z}\right)=\lambda\left(\frac{\partial^2 T}{\partial x^2}+\frac{\partial^2 T}{\partial y^2}+\frac{\partial^2 T}{\partial z^2}\right) \tag{5}$$

in this equation, c_p stands for the specific heat at constant pressure, λ indicates the fluid thermal conductivity, and T corresponds to the temperature of the fluid. The left-hand side of Eq. (5) depicts convective thermal transport induced by fluid motion, whereas the right-hand side stands for conductive heat transfer caused by temperature gradients.

2.2 Physical Model

Fig. 1 illustrates the three-dimensional structural schematic of the microchannel heat sink, primarily comprising a heat source and microchannels. The microchannel section primarily consists of an inlet buffer zone, an outlet buffer zone, and ten microchannels in between. The fluid medium enters the buffer zone through the inlet, undergoes buffering, and then flows uniformly into each microchannel for heat exchange. Finally, it converges in the outlet buffer zone before exiting through the outlet.

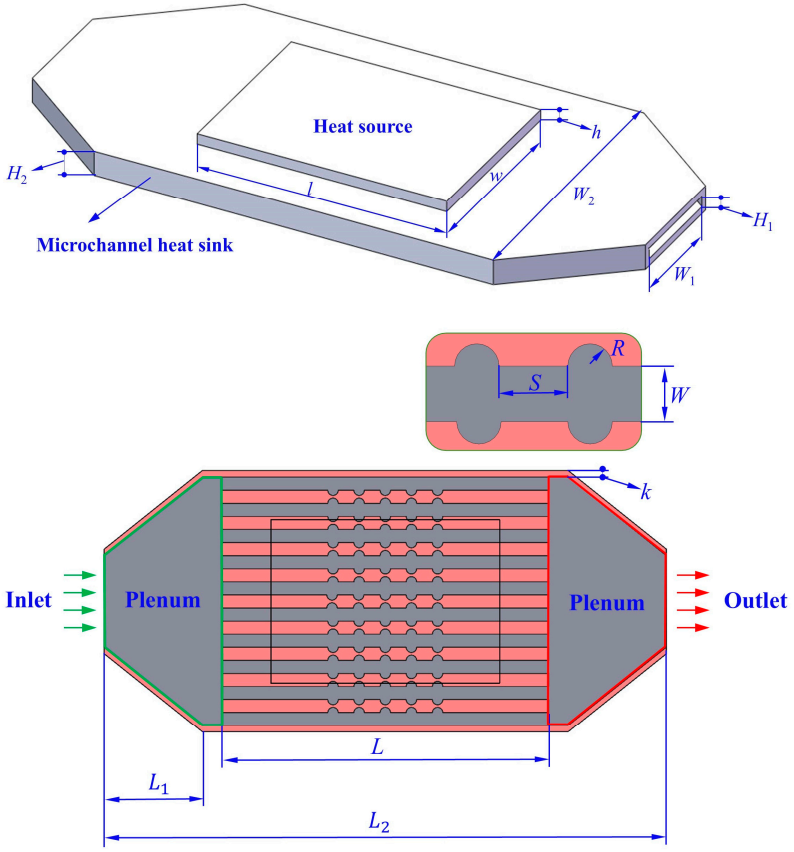

Figure 1: Schematic diagram of grooved microchannel heat sink.

The specific parameters of the geometric model are shown in Table 1.

Table 1: Structural parameters of microchannel heat sink.

Name	Value
Inlet/Outlet cross-section dimensions W1 × H1	14 mm × 1.5 mm
Input/Output buffer length L1	18 mm
Number of microchannels n	10
Microchannel spacing s	2 mm
Microchannel dimensions L × W × H	50 mm × 2 mm × 1.5 mm
Number of grooves N	0, 1, 3, 5, 7, 9, 11
Groove spacing S	1/2/2.4/3/4/5/6/mm
Groove dimensions R	0.8 mm
Shell thickness k	1 mm
Radiator Dimensions L2 × W2 × H2	86 mm × 40 mm × 3.5 mm
Heat source dimensions l × w × h	35 mm × 25 mm × 1.5 mm

2.3 Grid Partitioning

Generate a surface mesh using Fluent with the meshing component, then create the fluid domain. Subsequently, a boundary layer is arranged at the junction of fluid and solid computational domains. The simulation model employs a polyhedral mesh, generating 224,863 solid-domain and 199,486 fluid-domain meshes, totaling 424,349. The mesh orthogonality quality factor is 0.2, exceeding the 0.15 threshold. That indicates stable mesh quality, ensuring the numerical simulation remains stable. The overall and local mesh configurations of the simulation model after mesh partitioning are shown in Fig. 2, ((a) Local import grid partitioning of the microchannel region; (b) Overall mesh partitioning of the entire radiator; (c) Detailed mesh generation within the microchannels).

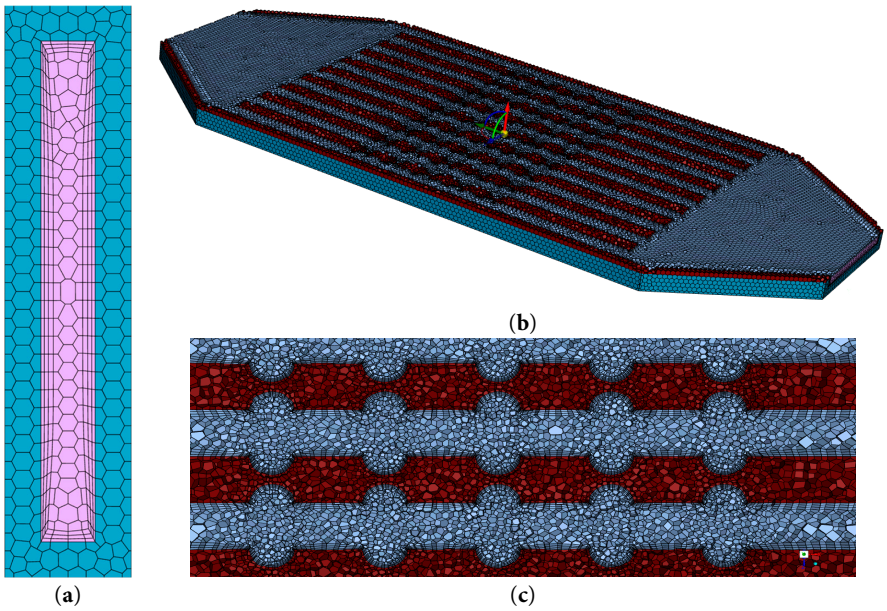

Figure 2: Grid partitioning schematic diagram: (**a**) Import grid partitioning; (**b**) Overall mesh partitioning of the radiator; (**c**) Mesh generation within microchannels.

The computational model was imported into the ANSYS Meshing platform for grid generation. To minimize numerical discrepancies and enhance computational precision, local mesh refinement within the fluid domain was implemented via the "Refine" function. Nevertheless, an elevated refinement level leads to a substantial increase in the number of mesh elements, thereby imposing more rigorous computational requirements. To verify the mesh independence of the solution, a specific case characterized by 5 grooves, a spacing of 2.4 mm, and an inlet velocity of 0.6 m/s was selected as the reference scenario; the grid convergence was systematically examined by adjusting the refinement levels ranging from 0 to 1. The test results are shown in Table 2.

Table 2: Grid independence test.

Refinement Level	Grid Number	Pressure Difference (Pa)	Relative Error	Average Temperature of the Heat Source (K)	Relative Error
0	152,918	652.21	17.01%	419.93	12.39%
1	260,336	611.31	9.69%	400.65	7.23%
2	424,349	572.2	2.66%	379.51	1.57%
3	678,958	557.4	—	373.64	—

As shown in Table 2, when the refinement level is set to 2, the relative error is 2.66% and 1.57%, respectively. Therefore, in this study, refinement level 2 is sufficient to meet the accuracy requirements.

2.4 Condition Settings

For the numerical simulation of groove-type microchannel heat sinks, the following assumptions are made:

(1) Assume single-phase flow heat transfer;
(2) Neglect the effects of thermal radiation and gravity [24–26];
(3) Assume the fluid is in laminar flow [27,28].

The finite volume method is adopted to simulate microchannel convective heat transfer. The Coupled implicit pressure-velocity coupling scheme is applied to solve continuity and momentum equations simultaneously, matching the pressure drop and flow-thermal coupling characteristics. For spatial discretization, cell-based least squares, second-order scheme and second-order upwind scheme are applied for gradient, pressure, momentum and energy terms respectively.

The cooling medium is set as liquid water with an inlet temperature of 283 K. Several distinct flow velocity values were adopted in the simulation, namely 0.6 m/s, 0.8 m/s, 1.0 m/s, 1.2 m/s, 1.4 m/s and 1.6 m/s. The outlet gauge pressure is 0 kPa, and backflow suppression is selected. Both the heat source and heat sink are made of copper. The heat flux at the heat source wall is 130 W/cm^2. Coupled boundary conditions are applied between internal flow channels, with a convective heat transfer coefficient set to 1800 W/(m^2·K).

The specific parameters for the boundary conditions and physical quantities mentioned above are listed in Table 3.

Table 3: Boundary condition name parameter settings.

Boundary Condition	Value	Boundary Type
Fluid medium	Water	Internal domain
Fluid inlet temperature T	283.15 (K)	Internal domain
Fluid inlet velocity v	0.6/0.8/1.0/1.2/1.4/1.6 (m/s)	Speed
Heat flux q	130 (W/cm^2)	/
Heat source and radiator structure	Copper	/
Convective heat transfer coefficient h	1800 W/(m^2·K)	/
Outlet gauge pressure p	0 (KPa)	Pressure
Inlet	/	Speed
Outlet	/	Pressure
Internal flow path	/	Wall
Heat source	/	Wall
Exterior wall surface	/	Wall

2.5 Evaluation Parameters

To assess the fluid flow behaviors and heat transfer properties of microchannels, a number of dimensionless parameters have been adopted. The formula for the Reynolds number (Re) is presented as follows:

$$Re = \frac{\rho_f u_m D_h}{\mu_f} \tag{6}$$

$$D_h = \frac{2WH}{(W+H)} \tag{7}$$

$$u_m = \frac{v W_1 H_1}{n W H} \tag{8}$$

where ρ_f denotes the density of the working fluid; u_m is the average inlet velocity for each individual microchannel; D_h represents the hydraulic diameter of the microchannel; μ_f stands for the dynamic viscosity of the working fluid.

The thermophysical properties of both water and copper are presented in Table 4. The calculated value of the Reynolds number are presented in Table 5.

Table 4: Physical properties of the material.

Thermophysical Property	Water	Copper
ρ (kg/m^3)	997	8978
λ (W/(m·K)	0.58	387.6
μ (kg/(m·s)	0.001308	-

Table 5: The calculated value of the Reynolds number.

Inlet Velocity v	0.6 m/s	0.8 m/s	1 m/s	1.2 m/s	1.4 m/s	1.6 m/s
Reynolds number	547	730	912	1095	1277	1459

To comprehensively assess the flow and heat transfer performance of microchannel structures, the performance evaluation criteria (PEC) are introduced. This criterion quantifies the synergistic relationship between heat transfer enhancement (characterized by Nu) and hydraulic penalty (represented by pressure drop), and is expressed as:

$$PEC = \left(\frac{Nu}{Nu_0}\right) / \left(\frac{f}{f_0}\right)^{1/3} \tag{9}$$

where Nu represents the Nusselt number of the target case, Nu_0 is the Nusselt number of the baseline reference case, f defines the friction factor of the target microchannel, and f_0 is the friction factor associated with the reference configuration.

The equation for the mean Nusselt number is presented below:

$$\mathrm{Nu} = \frac{h D_h}{\lambda_f} \tag{10}$$

$$h = \frac{q}{T_{w,avg} - T_{f,avg}} \tag{11}$$

where h denotes the mean convective heat transfer coefficient, q stands for the average heat flux across the fluid-solid interface, while $T_{w,avg}$ and $T_{f,avg}$ refer to the bulk-averaged wall temperature and fluid temperature, respectively. All the parameters discussed above all pertain to conditions within the microchannel region.

The simulated value of the friction coefficient (f) can be calculated using the following formula, which is derived from the Darcy–Weisbach formula:

$$f = \frac{2\Delta p D_\mathrm{h}}{\rho_\mathrm{f} L u_\mathrm{m}^2} \tag{12}$$

where, ΔP indicates the pressure drop, while L is the overall length of the microchannel structure.

Regarding the laminar flow in a rectangular cross-section microchannel, Shah proposed an expression for the average friction coefficient in the undeveloped flow regime:

$$fRe = 96(1 - 1.3553\alpha_c + 1.9467\alpha_c^2 - 1.7012\alpha_c^3 + 0.9563\alpha_c^4 - 0.2537\alpha_c^5) \tag{13}$$

where, α_c represents the aspect ratio of the channel, which is set to 1.33 in this paper; f represents the friction coefficient.

The temperature non-uniformity over the heating surface domain is quantitatively evaluated using the following metric:

$$\Delta T_{\text{non-uni}} = \frac{1}{2}\left(\left|T_{\max} - T_{\text{avg}}\right| + \left|T_{\min} - T_{\text{avg}}\right|\right) \tag{14}$$

where, $T_{\max}$ refers to the maximum temperature of the heating surface, $T_{\min}$ represents the minimum temperature, and T_{avg} stands for the average temperature of the heat source. A lower value of $\Delta T_{\text{non-uni}}$ indicates a more uniform thermal profile within the heat source region.

3 Results and Discussion

3.1 Effects of Working Fluid Velocity

A grooved microchannel with five grooves and a 2.4 mm interval was adopted. Six inlet velocities from 0.6 m/s to 1.6 m/s were set for comparison. The temperature variation patterns of the heat source, microchannel heat sink, and cooling working fluid were analyzed. The results are shown in Figs. 3 and 4 respectively.

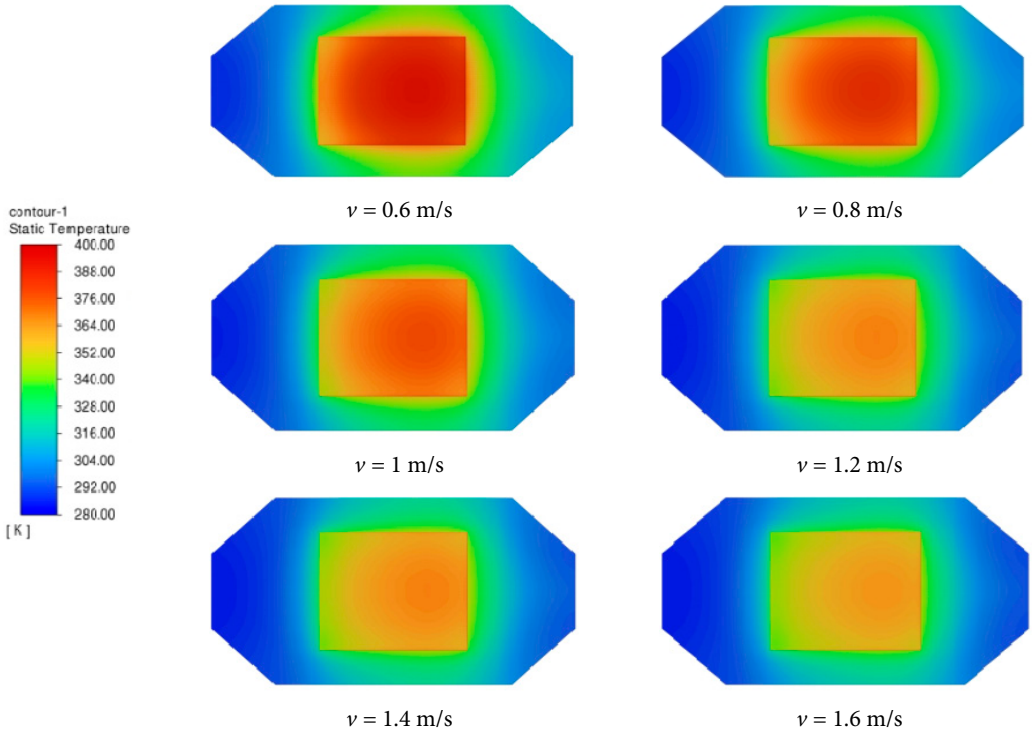

Figure 3: Temperature distribution of the heat source and microchannel heat exchanger at different flow rates.

Fig. 3 depicts the thermal distribution characteristics of the heat source and microchannel heat exchanger across different flow conditions. As the working fluid velocity increases, the maximum temperature of the heat source decreases significantly, and the high-temperature region of the microchannel heat exchanger shrinks.

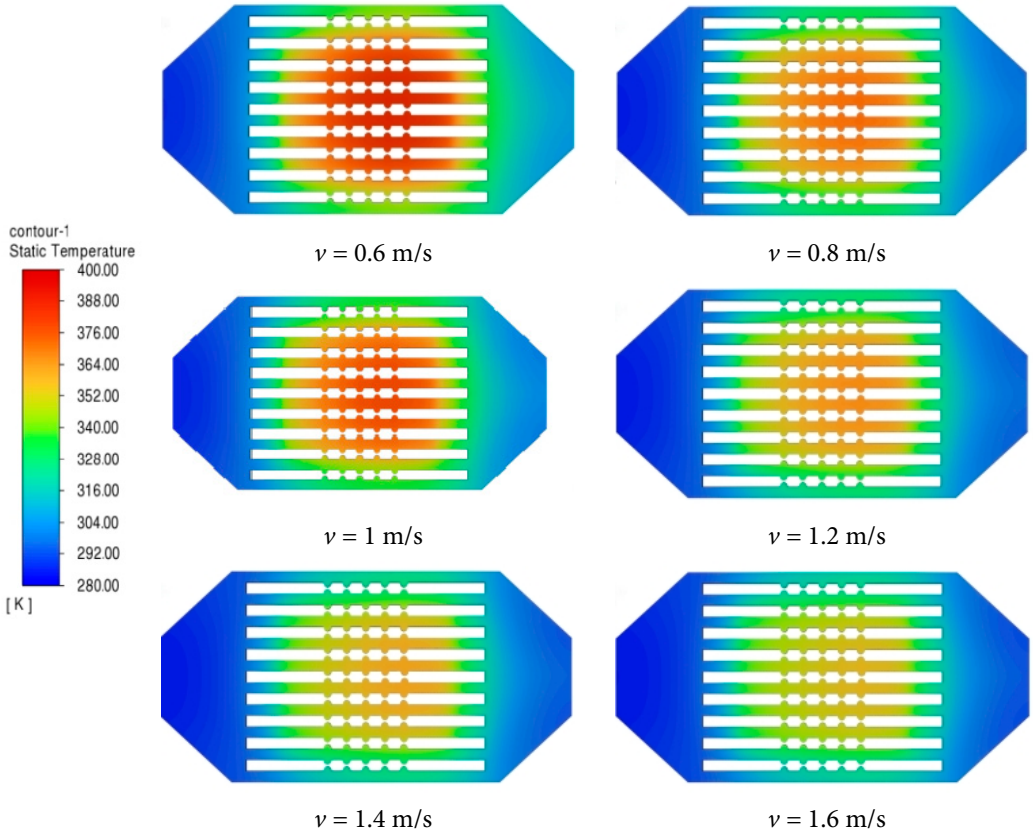

Figure 4: Temperature distribution of the working fluid at different flow rates.

Fig. 4 illustrates the temperature field characteristics of the working fluid across different flow conditions. As the working fluid flow rate increases, the outlet temperature decreases significantly.

As shown in Fig. 5, both the heat source temperature and the working fluid outlet temperature decrease with increasing flow velocity. Analysis reveals the following mechanism: the high-temperature heat source transfers heat to the microchannel wall by conduction, and the cooling working fluid subsequently removes heat from the wall by convective heat transfer. Increased fluid velocity within the microchannel elevates the flow Reynolds number. Increased turbulence intensifies the disruption of the thermal boundary layer, which further reduces thermal resistance and thereby enhances the intensity of convective heat transfer. Consequently, heat generated by the heat source is rapidly transferred through the microchannel wall into the working fluid, preventing heat accumulation at the source and thereby lowering its temperature.

Meanwhile, under conditions where the structural dimensions of the microchannel remain unchanged, higher inlet velocity directly decreases the residence time of the working fluid in the microchannel, reducing heat accumulation. This prevents the working fluid from being sufficiently heated within the channel, consequently lowering the outlet temperature. This effect helps maintain a larger temperature difference across the heat transfer surface, thereby enhancing the heat transfer rate. Furthermore, an increase in flow velocity directly results in a higher mass flow rate of the working fluid through the microchannel, thereby

increasing the total heat absorption. Research indicates that increased flow velocity enhances convective heat transfer within microchannels while reducing thermal resistance. Concurrently, the increased working fluid flow rate and reduced residence time significantly increase the heat extraction rate from the heat source, mitigating the temperature rise in the working fluid. That ultimately achieves simultaneous reductions in both the heat source temperature and the working fluid outlet temperature.

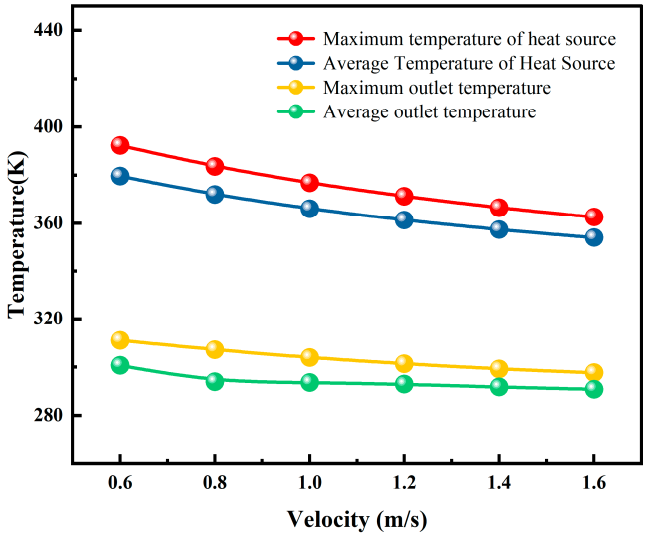

Figure 5: Variation of temperature with fluid velocity at different temperatures.

To more accurately investigate the effects of flow velocity on flow and heat transfer in grooved microchannels, the following analysis will focus solely on how the pressure drop, friction factor, temperature non-uniformity, Nusselt number, and PEC within the microchannel region vary with changes in the Reynolds number.

Fig. 6 illustrates the variation of pressure drop (Δp) within the microchannel region as a function of the Reynolds number (Re). As observed from the plot, the pressure difference between the microchannel inlets and outlets increases approximately linearly with the rise of the Reynolds number. The Reynolds number is directly proportional to the inlet flow velocity; higher velocity of the working medium significantly increases the inertial forces and wall shear stresses acting on the fluid within the microchannel. At the same time, the grooved structure exacerbates secondary flow and boundary layer separation, further increasing flow resistance, which ultimately causes the pressure drop to increase in tandem with the Reynolds number.

Fig. 6 presents a comparison between the theoretical laminar flow results for rectangular microchannels (calculated via Shah's equation) and the measured friction coefficient (f) of the groove-type microchannels. With an increase in the Reynolds number, the friction factor exhibits an initial sharp decline followed by a gradual decrease. Specifically, as the Reynolds number rises from 547 to 1459, the friction coefficient of the grooved microchannel decreased from 0.121 to 0.065, a reduction of 46.2%. In terms of the patterns of change, the overall trend of the simulated values is in complete agreement with the theoretical results for laminar flow in rectangular microchannels: within the laminar range, the friction coefficient decreases as the Reynolds number increases, and the rate of decrease gradually slows down at high Reynolds numbers.

It is worth noting that the friction coefficients of grooved microchannels are all higher than the theoretical values for smooth rectangular microchannels. This is because the grooved structure disrupts the stability of the boundary layer on the channel walls, inducing vortical disturbances and secondary flow within the fluid, which significantly increases local flow resistance and energy loss. Although the rate

of increase in pressure drop slows as the Reynolds number rises, the additional resistance caused by the grooves persists, resulting in a friction coefficient that remains higher than that of smooth rectangular microchannels. At the same time, the discrepancy between the simulation results and Shah's equation confirms the significant influence of the grooved structure on flow characteristics, providing data support for subsequent structural optimization.

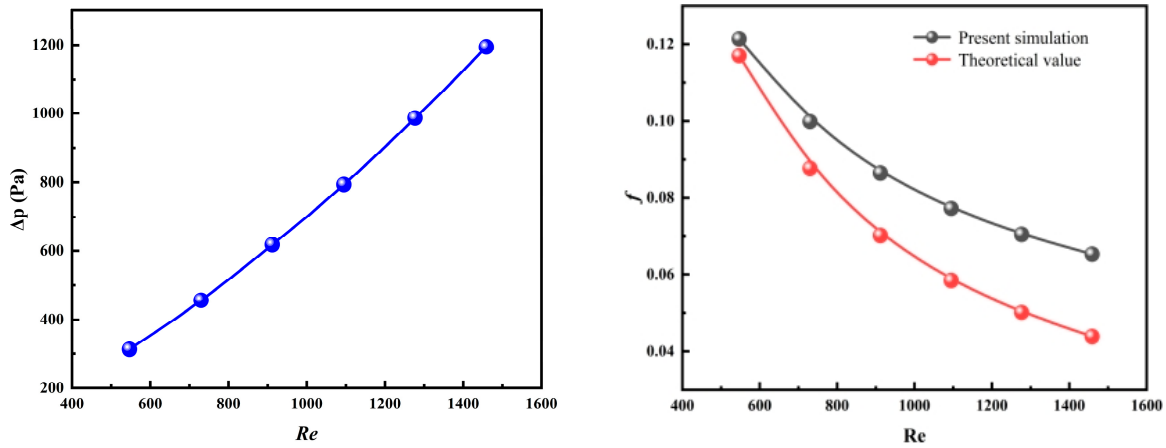

(**a**) Δp (**b**) f

Figure 6: Variations of (**a**) Δp, and (**b**) f with Re.

Fig. 7a shows how the average *Nu* changes with *Re* for the grooved microchannel. As observed in the figure, the average *Nu* increases with the *Re* throughout the investigated range of *Re* = 547 to 1459. This trend is consistent with the results reported in Reference [23], confirming the reliability of the numerical simulation. The Reynolds number is directly proportional to the inlet flow velocity; an increase in flow velocity significantly enhances the intensity of fluid turbulence within the microchannel, effectively disrupting the thermal boundary layer attached to the wall and reducing its thickness. This substantially lowers the convective heat transfer resistance and improves heat transfer performance, ultimately resulting in a continuous increase in the average Nusselt number.

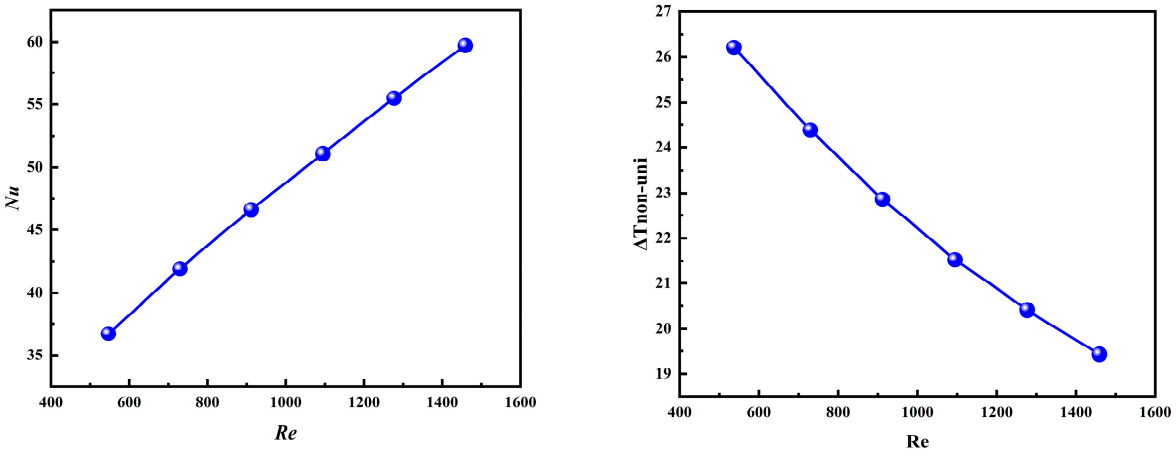

(**a**) *Nu* (**b**) $\Delta T_{\text{non-uni}}$

Figure 7: Variations of (**a**) *Nu*, and (**b**) $\Delta T_{\text{non-uni}}$ with *Re*.

The variation of heat source temperature non-uniformity ($\Delta T_{\text{non-uni}}$) with *Re* is plotted in Fig. 7b. The results indicate that heat source temperature non-uniformity decreases as the Reynolds number increases. Within the investigated range of Reynolds numbers (547–1459), $\Delta T_{\text{non-uni}}$ decreased from approximately 26.2°C to approximately 19.3°C, a reduction of 26.3%. Based on the trend shown in Fig. 7a, it can be concluded that increasing the Reynolds number offers a twofold benefit: the average Nusselt number increases significantly, thereby improving overall heat transfer performance, while at the same time the temperature uniformity of the heat source is significantly enhanced. This is because the convective heat transfer capacity of the fluid increases at high flow rates, allowing heat to be rapidly removed from all areas of the heat source. This prevents localized heat buildup, thereby reducing the difference between the maximum and average temperatures of the heat source and resulting in a more uniform temperature distribution.

In summary, increasing the Reynolds number (i.e., increasing the inlet flow velocity) can simultaneously achieve the dual effects of enhancing heat transfer performance and optimizing temperature uniformity, thereby providing a clear theoretical basis for optimizing the operating conditions of grooved microchannel heat sinks.

To quantitatively evaluate the overall heat dissipation performance of grooved microchannels under different inlet flow velocities, this paper employs the Performance Evaluation Criterion (*PEC*) to perform a trade-off analysis between heat transfer capacity and flow resistance. The calculation results as a function of the Reynolds number (*Re*) are shown in Fig. 8.

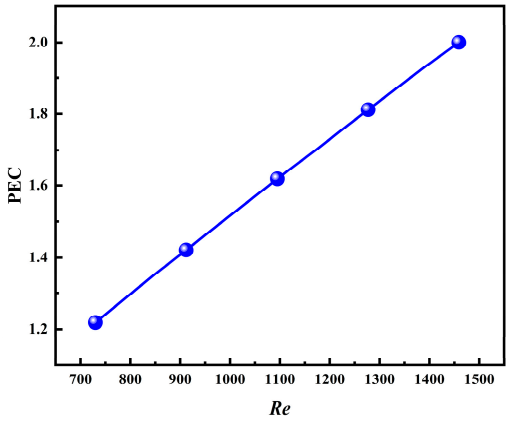

Figure 8: Variations of *PEC* with *Re*.

As can be seen from the Fig. 8, within the Reynolds number range studied (*Re* = 547~1459), the PEC value exhibits an increasing trend as the Reynolds number rises. As the Reynolds number increased from 547 to 1459, the *PEC* value rose from 1.22 to 2.05, representing an increase of 68.0%. This principle indicates that, although increasing the flow velocity leads to a significant increase in pressure drop and friction coefficient within the microchannel (resulting in greater flow resistance), the improvement in heat transfer performance far outweighs the increase in resistance.

Based on the previous analysis of the Nusselt number and pressure drop, it can be seen that the enhanced convective heat transfer resulting from increased flow velocity (a significant increase in the Nusselt number) effectively offsets the energy loss caused by the rise in pressure drop, ultimately leading to continuous optimization of the overall heat dissipation performance of the grooved microchannels. These results further confirm that, within the operating conditions considered in this study, increasing the inlet flow velocity is an effective strategy for enhancing the overall performance of grooved microchannel

heat sinks, providing important guidance for selecting operating conditions in engineering applications involving high heat flux scenarios.

3.2 Effect of Groove Quantity

Set groove count N = 0/1/3/5/7/9/11. Under conditions of working fluid inlet velocity v = 0.8 m/s and groove spacing S = 2.4 mm, simulations were conducted to investigate the effect of disturbance unit count on microchannel heat dissipation performance. Temperature variation patterns for the heat source, the microchannel heat sink, and the cooling working fluid are shown in Figs. 9–11 respectively.

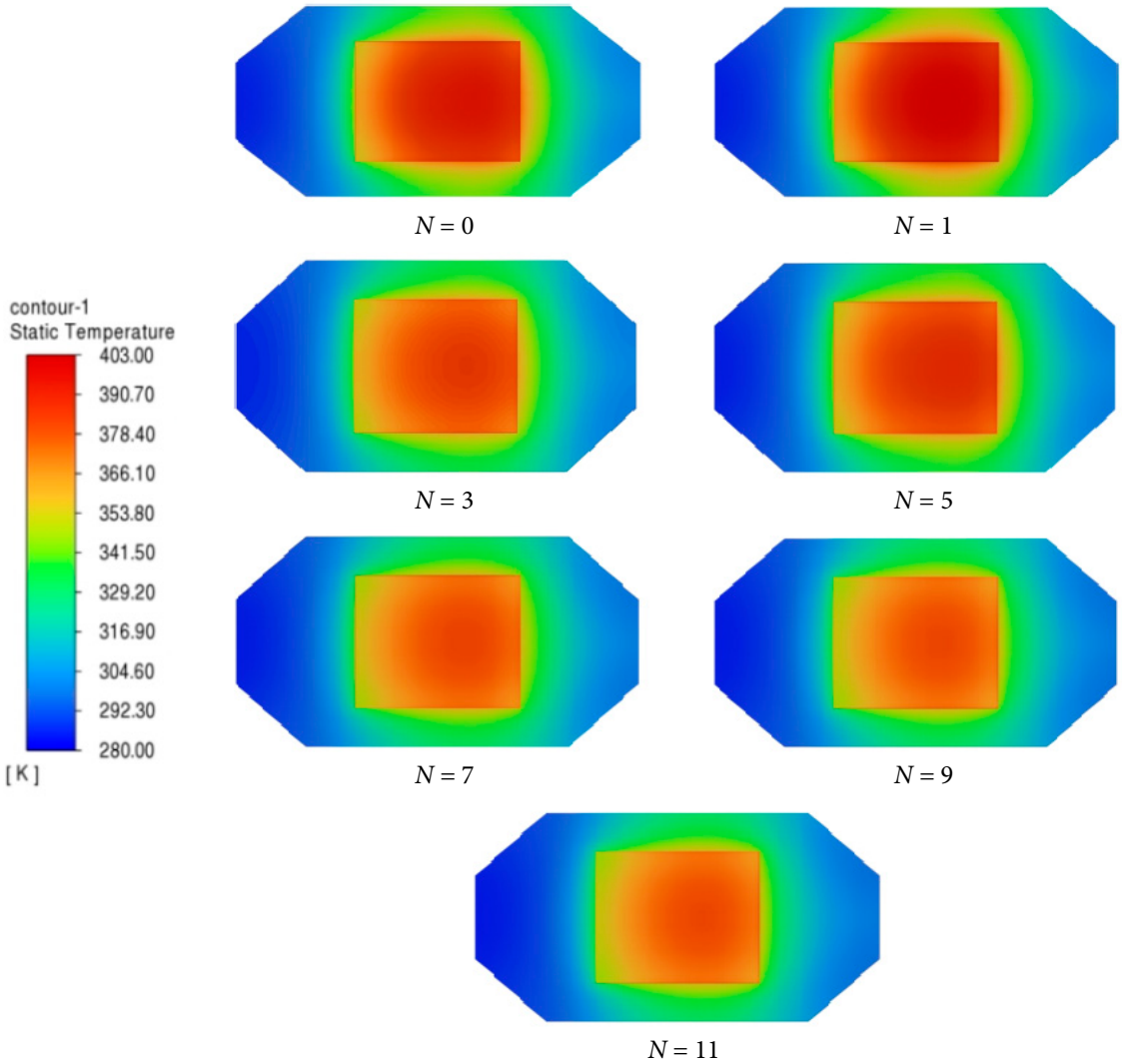

Figure 9: Temperature distribution of heat sources and heat sinks at different groove counts.

Fig. 9 displays the temperature field characteristics of the heat source and heat sink across different groove configurations. The results show that a gradual increase in the number of grooves leads to both a contraction of the heat sink's high-temperature region and a notable drop in the heat source's peak temperature. When N = 0 (smooth channel), the high-temperature zone is the largest, and the center temperature is the highest; When N = 1, the high-temperature zone shrinks significantly, and the temperature decreases. As N increases from 3 to 11, the high-temperature zone gradually shrinks.

As presented in Fig. 10, the thermal distribution of the working fluid is shown for different groove numbers. Even with a gradual increase in the number of grooves, the working fluid outlet temperature remains nearly constant.

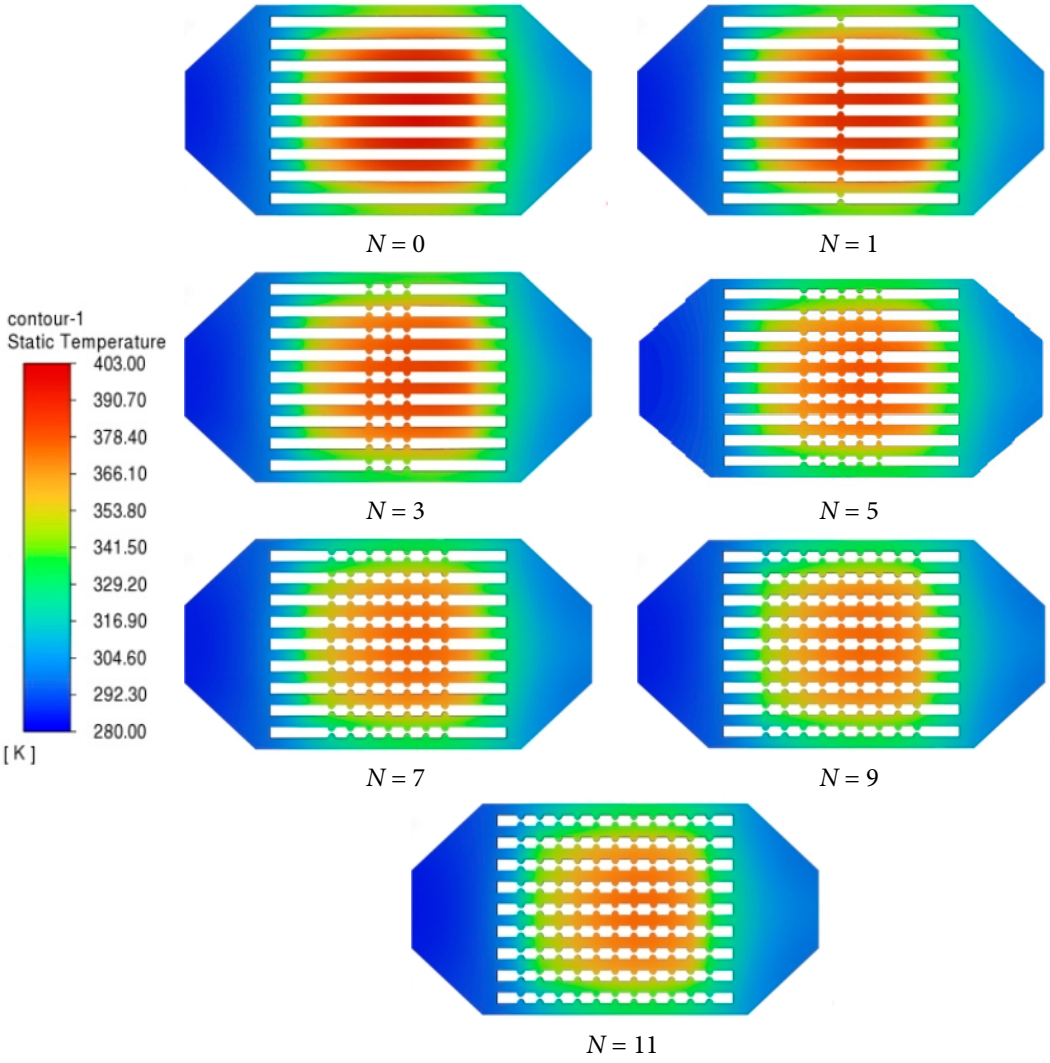

Figure 10: Distribution of fluid temperature at different groove counts.

Fig. 11 shows how the heat source and fluid temperatures vary with the number of grooves. Grooves, as typical passive heat transfer enhancement structures within microchannels, disrupt the working fluid's laminar boundary layer (see Fig. 12 ((a) Overall flow distribution across the full radiator; (b) Partial flow distribution in the microchannel array; (c) Detailed flow distribution within a single microchannel); Fig. 13 ((a) Overall flow distribution across the full radiator; (b) Partial flow distribution in the microchannel array; (c) Detailed flow distribution within a single grooved microchannel), inducing recirculation and vortex motion in the groove region. That significantly enhances mixing between the near-wall fluid and the main flow zone. Moreover, a higher number of grooves increases the density of disturbance points within the channel, leading to a marked improvement in the local convective heat transfer coefficient. On the other hand, the groove structure increases the actual effective heat exchange area of the microchannel, with the heat exchange area expanding in tandem as the number of grooves increases. Research indicates that

increasing the number of grooves within microchannels can effectively enhance convective heat transfer rates between heat sources and working fluids, thereby reducing heat source temperatures and improving thermal reliability. However, as the number of grooves increases, the marginal effect diminishes. The marginal effect is greatest when increasing from N = 0 to N = 1, significantly declines when increasing from N = 1 to N = 5, and approaches zero when increasing from N = 7 to N = 11.

Fig. 14 presents the velocity vector plots for different groove numbers, which visualize the flow structures and vortex formation within the microchannel. As the groove number increases, recirculation vortices appear within the grooves, as indicated by the local eddy patterns in the vector field. These vortices disrupt the laminar flow and enhance transverse mixing, which breaks the thermal boundary layer and promotes convective heat transfer.

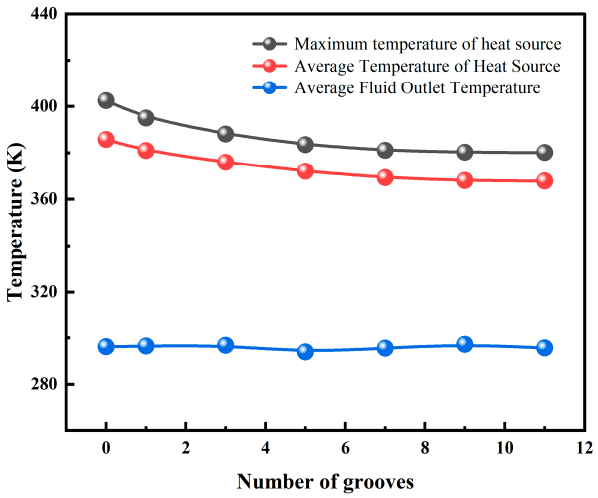

Figure 11: Temperature variation with number of grooves.

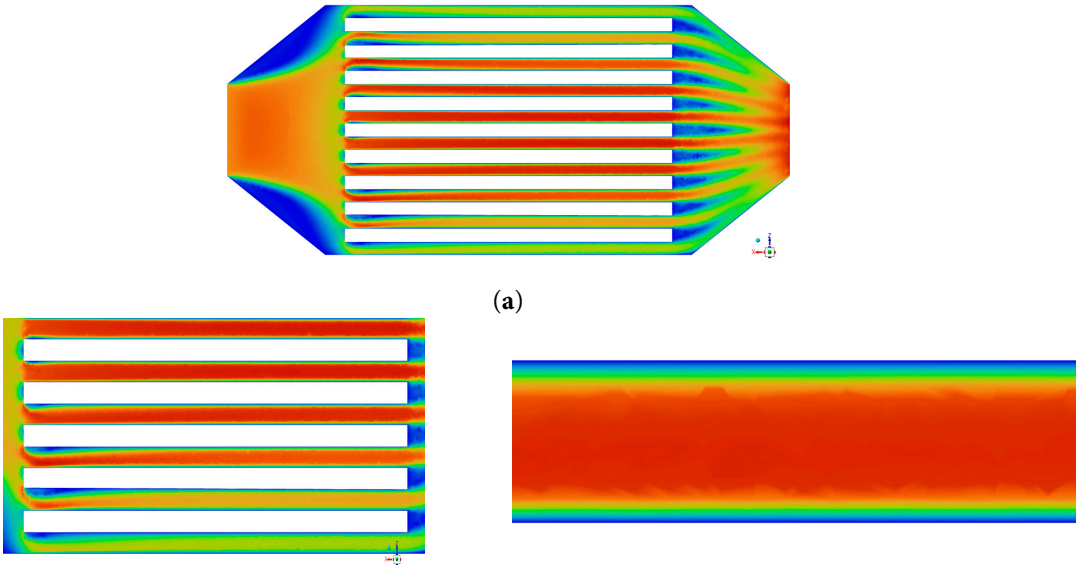

Figure 12: Flow distribution diagram without grooves. (**a**) Overall flow distribution diagram; (**b**) Partial flow distribution diagram; (**c**) Flow distribution diagram for a single flow channel.

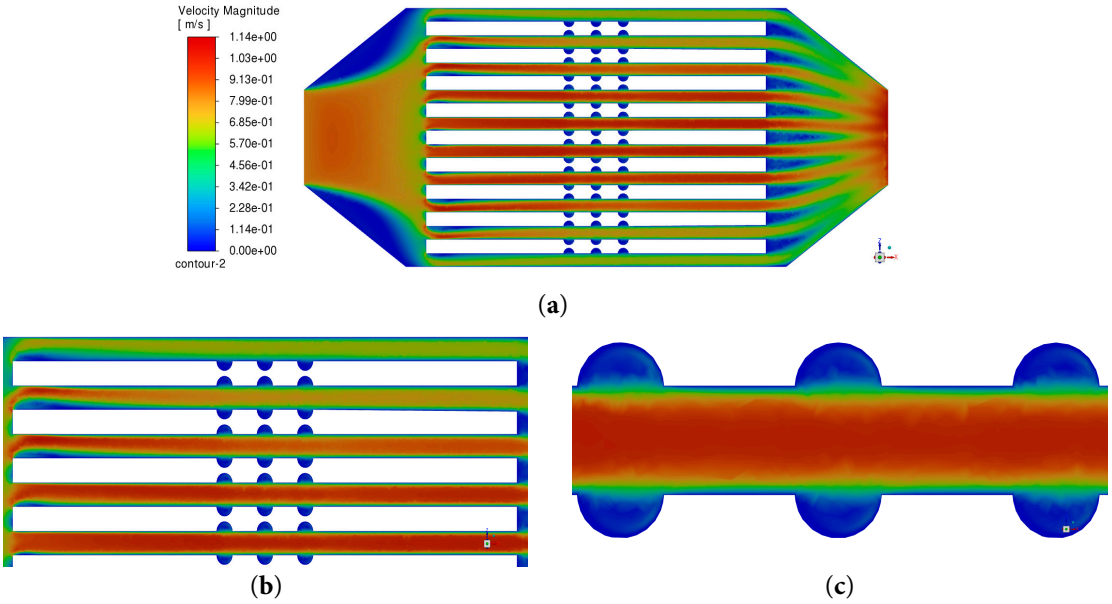

Figure 13: Grooved flow distribution diagram. (**a**) Overall flow distribution diagram; (**b**) Partial flow distribution diagram; (**c**) Flow distribution diagram for a single flow channel.

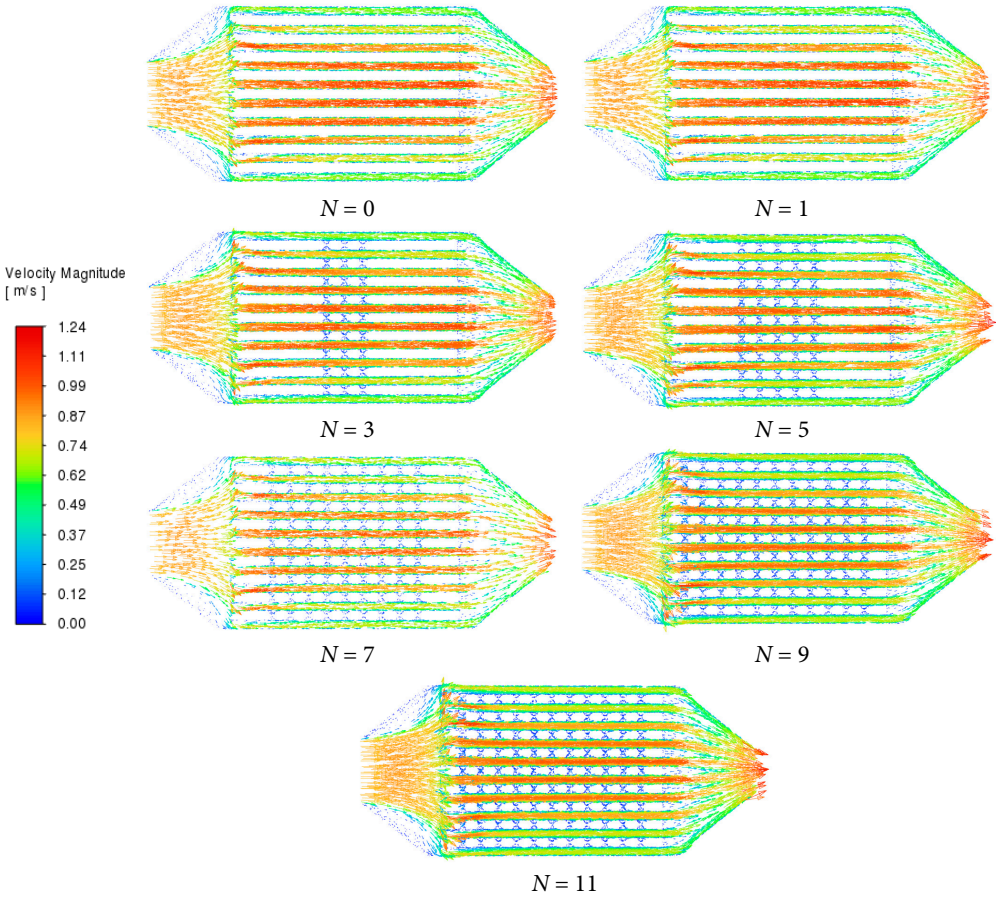

Figure 14: Velocity vector plots for different numbers of grooves.

The fluid outlet temperature remains nearly constant with increasing groove number, which can be rigorously explained from the first law of thermodynamics (global energy conservation). For the present system, the total heat input rate q_w is fixed, and the working fluid mass flow rate $\dot{m}$, specific heat capacity c_p, and inlet temperature T_{in} are all prescribed as constant boundary conditions. The steady-flow energy balance yields:

$$q_{\text{w}} = \dot{m} c_p (T_{\text{out}} - T_{\text{in}}) \tag{15}$$

Since q_w, $\dot{m}$, c_p, and T_{in} are independent of the groove configuration, the outlet temperature T_{out} is uniquely determined and must remain constant regardless of the number of grooves. This conclusion follows directly from the first law and holds irrespective of internal flow details, local thermal non-uniformities, or the degree of convective enhancement.

While the outlet temperature is invariant, increasing the groove number significantly alters the local temperature field within the solid and fluid domains. The additional grooves disrupt the thermal boundary layer, promote flow mixing, and enhance local convective heat transfer coefficients. These effects do not change the total energy absorbed by the fluid but redistribute the thermal resistance, resulting in a significantly more homogeneous temperature field on the heat source and a reduction in its maximum temperature. From a thermodynamic perspective, the increased groove number increases internal irreversibilities (entropy generation) due to enhanced mixing and flow disturbance, yet the global energy balance remains unchanged. Thus, the observed invariance of outlet temperature is a direct consequence of global energy conservation, while the improved thermal performance manifests in local temperature uniformity and reduced peak temperatures.

To more accurately elucidate the influence of the number of grooves on the flow and heat transfer characteristics of microchannels, this section systematically analyzes the variation of pressure drop (Δp), friction factor (f), temperature non-uniformity, Nusselt number (Nu), and the comprehensive performance evaluation factor (PEC) with respect to the number of grooves under a fixed Reynolds number (Re = 730).

The variation in the pressure drop between the microchannel inlet and outlet with different groove configurations is plotted in Fig. 15a. As shown in the figure, within the range of groove numbers studied (N = 0~11), the pressure drop in the microchannel exhibits a monotonically increasing trend as the number of grooves increases, and the rate of increase gradually slows down as the number of grooves increases. Under steady-state conditions with Re = 730, as the number of grooves increased from 0 (smooth rectangular microchannel) to 11, the pressure drop rose from 416.16 Pa to 483.00 Pa, representing an increase of 16.05%. This is because the grooved structure disrupts the stability of the boundary layer on the channel walls, inducing vortical disturbances and secondary flow within the fluid, thereby increasing local flow resistance and energy loss; the greater the number of grooves, the larger the scope and intensity of the fluid disturbances, and the more pronounced the cumulative effect on flow resistance, ultimately leading to a continuous increase in pressure drop.

Fig. 15b shows the variation of the microchannel friction coefficient as a function of the number of grooves. The results indicate that the trend in the friction coefficient aligns with that of the pressure drop: it increases as the number of grooves increases, and the rate of increase gradually slows down at higher groove counts. As the number of grooves increased from 0 to 11, the coefficient of friction rose from 0.0911 to 0.1056, representing an increase of 15.92%. This finding further confirms the role of grooved structures in enhancing flow resistance.

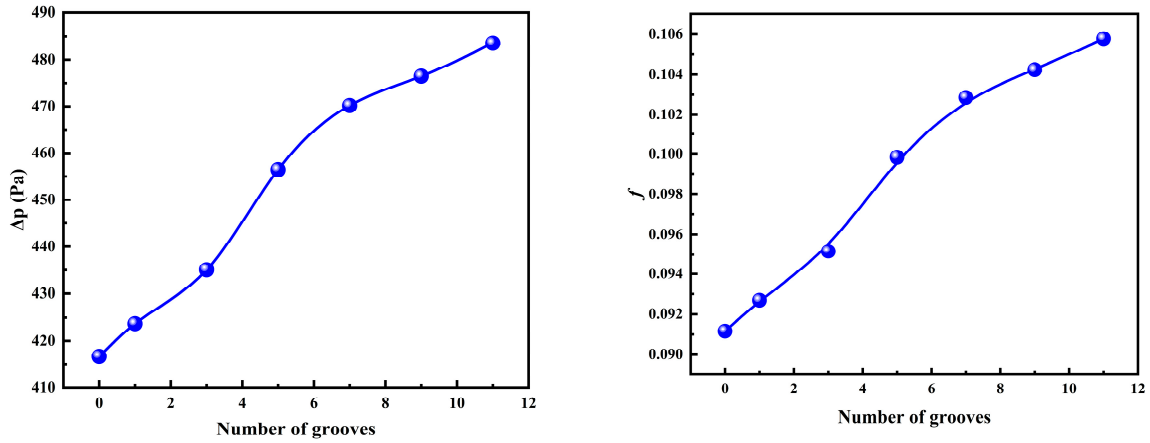

(**a**) Δp (**b**) f

Figure 15: Variations of (**a**) Δp, and (**b**) f with the number of grooves.

To further clarify the effect of the number of grooves on the heat transfer performance and temperature uniformity of microchannels, Fig. 15a,b shows the variation of the average Nusselt number and heat source temperature non-uniformity with respect to the number of grooves, respectively.

As shown in Fig. 16a, the average Nusselt number increases as the number of grooves increases, and the rate of increase gradually slows down as the number of grooves increases. Smooth microchannels without grooves have the lowest average Nusselt number, at just 31.8; when the number of grooves is increased to 11, the Nusselt number rises to 46.9, representing a 47.5% increase compared to smooth channels. This indicates that the grooved structure enhances heat transfer in microchannels; however, once the number of grooves exceeds a certain threshold, its effect on disrupting the thermal boundary layer tends to plateau, and the marginal benefit of heat transfer enhancement gradually decreases. Fig. 16b shows the curve of the temperature non-uniformity of the heat source as a function of the number of grooves. It can be concluded that increasing the number of grooves contributes to a rapid reduction in the heat source's temperature unevenness in the initial stage, followed by a subsequent upward trend.

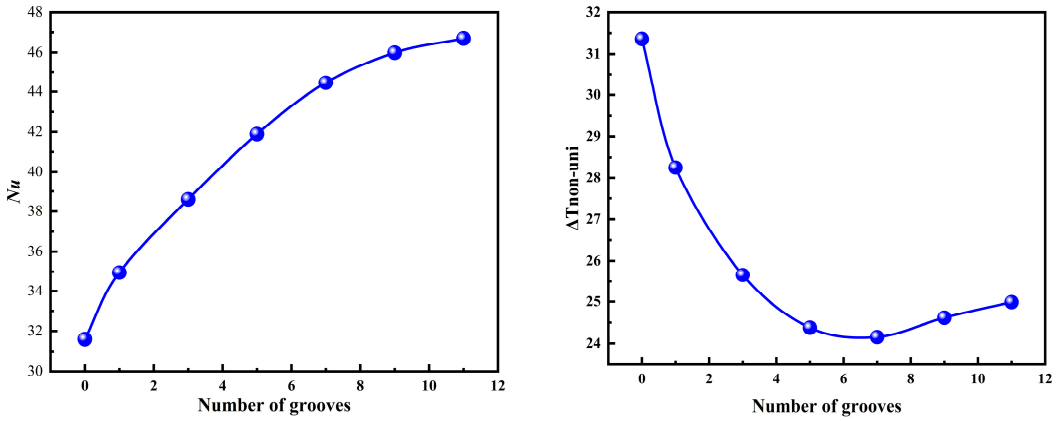

(**a**) Nu (**b**) $\Delta T_{\text{non-uni}}$

Figure 16: Variations of (**a**) Nu, and (**b**) $\Delta T_{\text{non-uni}}$ with the number of grooves.

Fig. 17 shows the variation of the comprehensive performance evaluation factor PEC with the number of grooves; all calculations are nondimensionalized using a smooth rectangular microchannel as a reference.

As shown in the figure, *PEC* exhibits an upward trend as the number of grooves increases, but the rate of increase gradually slows down as the number of grooves rises. For a smooth channel without grooves, the *PEC* is 1.0; when the number of grooves is increased to 8, the *PEC* rises to 1.39, a 39% increase over the smooth channel; when the number of grooves is further increased to 11, the *PEC* rises only slightly to 1.405, an increase of less than 1.1%. These results indicate that grooved structures can effectively enhance the overall flow and heat transfer performance of microchannels; however, as the number of grooves increases, the marginal benefit of this performance improvement gradually decreases. Combining the preceding analysis of the Nusselt number and pressure drop reveals that when the number of grooves is small, the heat transfer enhancement resulting from adding grooves (a significant increase in the Nusselt number) far outweighs the increase in flow resistance, causing the *PEC* to rise rapidly. However, when the number of grooves exceeds 8, the marginal benefit of heat transfer enhancement diminishes, while flow resistance continues to accumulate, leading to a significant slowdown in the rate of increase of the *PEC*. This finding also supports the conclusion reached earlier: under operating conditions of Re = 730, setting the number of grooves to 8 achieves an optimal balance between heat transfer enhancement, temperature uniformity, and flow resistance. Further increasing the number of grooves has only a limited effect on improving overall performance, while actually increasing manufacturing costs and flow energy consumption.

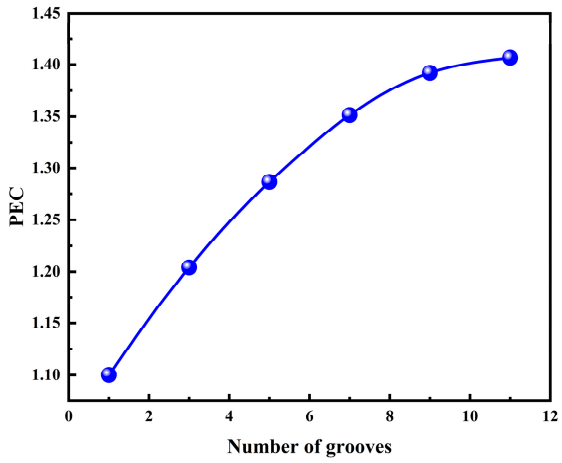

Figure 17: Variations of *PEC* with the number of grooves.

3.3 Effect of Groove Spacing

As discussed earlier, incorporating grooves within the microchannel can enhance the heat dissipation performance of microchannel heat sinks. Under fixed boundary conditions (groove radius R = 0.8 mm, groove height H = 1.5 mm, heat flux density q = 130 W/cm^2, working fluid inlet temperature T = 10°C, flow velocity v = 0.8 m/s), microchannel heat dissipation performance simulations were conducted by varying only the groove spacing S across six conditions: 1 mm, 2 mm, 3 mm, 4 mm, 5 mm, and 6 mm.

Fig. 18 shows the temperature distribution of the heat source and heat sink at different groove spacings. When the groove spacing is 1 mm, 2 mm, 3 mm, 4 mm, 5 mm, and 6 mm, respectively, the high-temperature zones are extremely concentrated, slightly dispersed, noticeably dispersed, further dispersed, and most extensive.

Fig. 19 shows the fluid temperature distribution at different groove spacings. When the groove spacing is small (S = 1 mm), temperature stratification occurs, with the high-temperature zone concentrated near the wall surface. At a moderate groove spacing (S = 3 mm), the temperature distribution becomes uniform,

and the high-temperature zone extends toward the center of the flow channel. When the groove spacing is large (S = 6 mm), temperature stratification reappears.

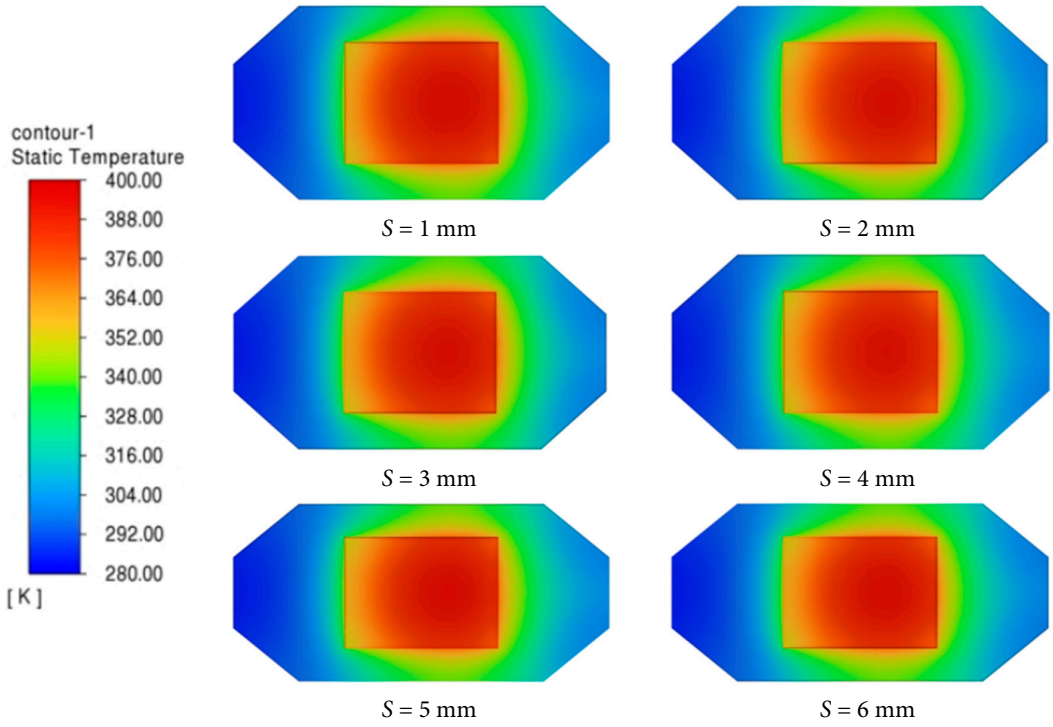

Figure 18: Temperature distribution of heat sources and heat sinks at different groove spacings.

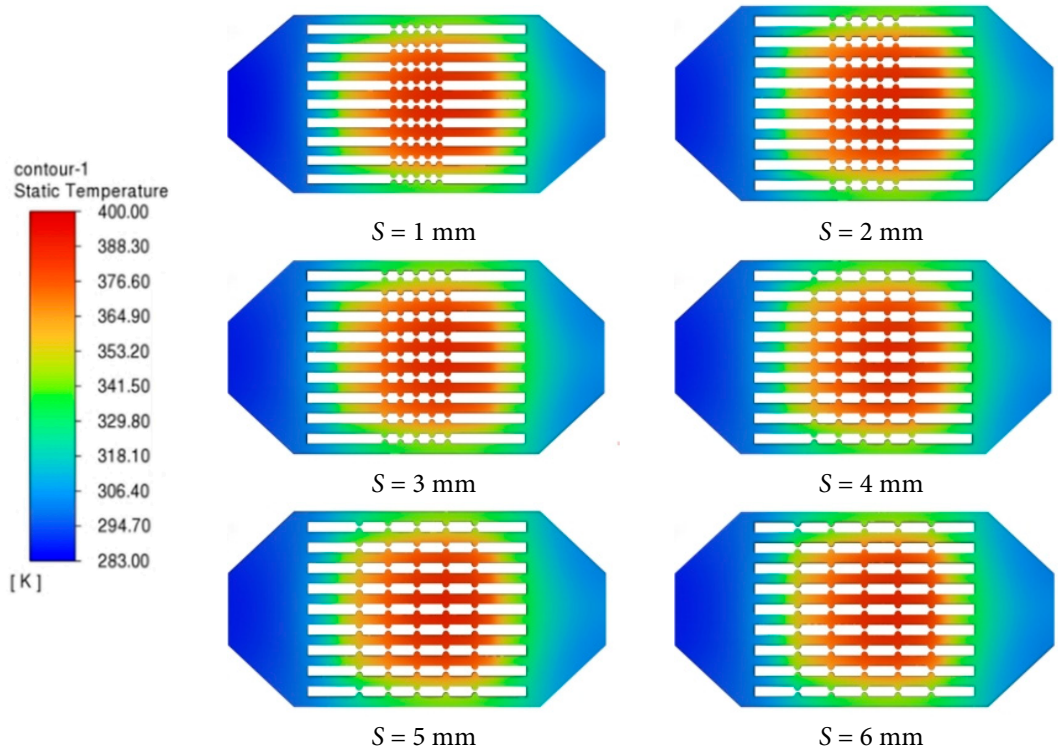

Figure 19: Distribution of fluid temperature at different groove spacings.

As illustrated in Fig. 20, with the gradual enlargement of groove spacing, the highest temperature of the heat source presents a trend of initial reduction followed by elevation. The optimal condition with the lowest central temperature appears at S = 3 mm. When groove spacing is small (1–2 mm), flow obstruction reduces the heat transfer coefficient; simultaneously, vortex interference creates localized hot spots. Among the groove spacings considered in this study, the configuration with 3 mm spacing yields the lowest heat source temperature. At this spacing, eddy currents develop fully without excessive interference, resulting in minimal thermal resistance and maximum heat transfer coefficient under the present geometric and operating conditions. When the groove spacing is large (5–6 mm), the boundary layer fully develops, leading to a decrease in the heat transfer coefficient.

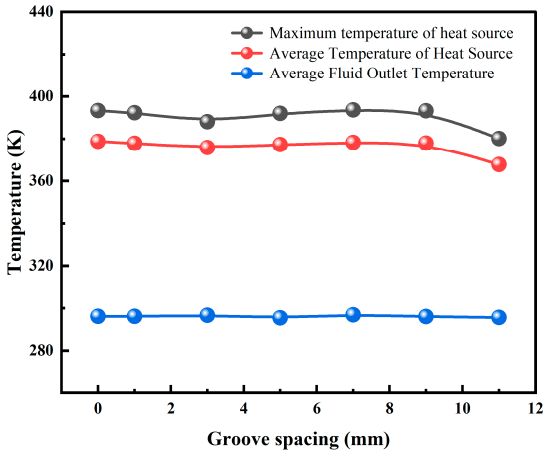

Figure 20: Temperature variation with groove spacing.

To further clarify the influence of groove spacing on the flow and heat transfer characteristics of microchannels, we will systematically analyze how the pressure drop, friction factor, temperature non-uniformity, Nusselt number, and the comprehensive performance evaluation factor *PEC* vary with changes in groove spacing within the microchannel region.

Fig. 21a shows the variation of the pressure drop at the microchannel inlet and outlet as a function of groove spacing. As shown in the figure, the pressure drop first increases and then decreases as the groove spacing increases. Fig. 21b shows the variation of the microchannel friction coefficient as a function of groove spacing. As can be seen, the trend in the friction coefficient is consistent with that of the pressure drop.

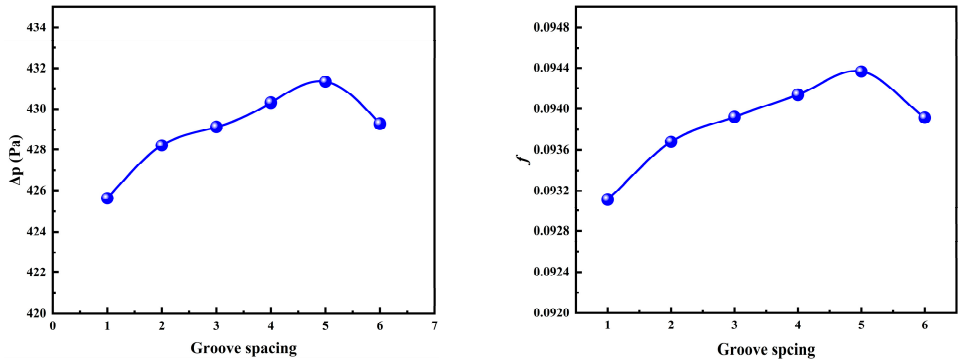

(**a**) Δp (**b**) f

Figure 21: Variations of (**a**) Δp, and (**b**) f with the spacing of groove.

The influence of the groove spacing on the heat transfer performance of the microchannel and the temperature uniformity of the heat source is presented in Fig. 22a,b. As can be seen from Fig. 22a, as the groove spacing increases, the average Nusselt number presents an initial upward trend followed by a gradual reduction. Fig. 22b shows the variation curve of the heat source temperature non-uniformity with the groove spacing. Overall, the fluctuation range of is relatively small, varying only within the range of 28.0–29.2°C, indicating that the influence of the groove spacing on the temperature uniformity of the heat source is relatively limited.

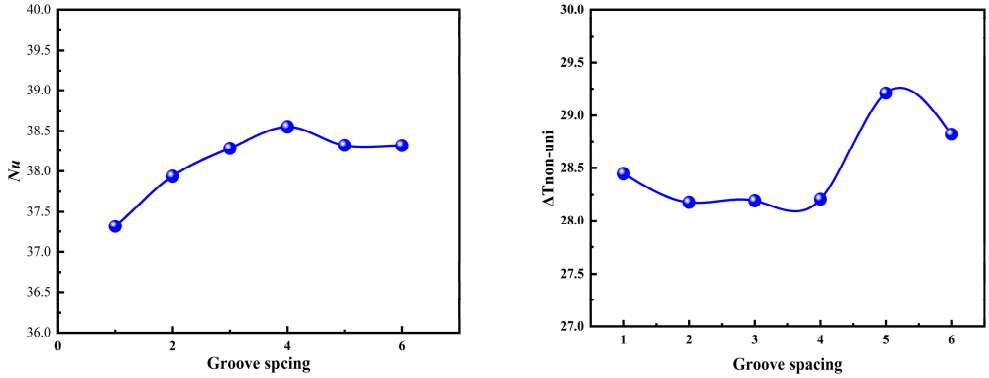

(**a**) *Nu* (**b**) $\Delta T_{\text{non-uni}}$

Figure 22: Variations of (**a**) *Nu*, and (**b**) $\Delta T_{\text{non-uni}}$ with the spacing of groove.

To quantitatively evaluate the comprehensive flow and heat transfer performance of microchannels with different groove spacings, this paper conducts non-dimensionalization based on a smooth rectangular microchannel and calculates the comprehensive performance evaluation factor *PEC*. As shown in Fig. 23, the *PEC* value first increases, then decreases, and then slightly rebounds as the groove spacing increases. In summary, within the parameter range studied in this paper, a groove spacing of 3 mm can achieve an optimal balance between heat transfer enhancement and flow resistance, and it is the optimal structural parameter for the grooved microchannel under the current working conditions.

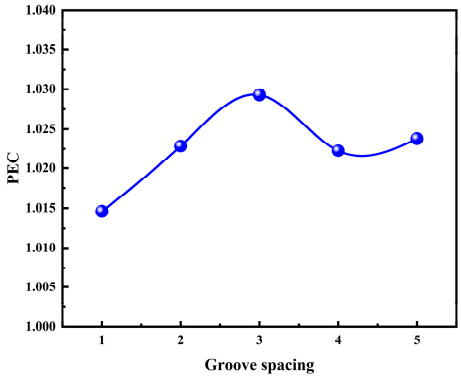

Figure 23: Variations of *PEC* with the spacing of groove.

4 Conclusion

This paper employs computational fluid dynamics and heat transfer theory to conduct a comprehensive analysis of factors affecting the heat dissipation performance of groove-type microchannel heat exchangers through numerical simulation. The main conclusions are as follows:

(1) Increasing the inlet flow velocity of the working fluid can significantly enhance the heat dissipation capacity of grooved microchannels. As the Reynolds number increases, both the heat source temperature and the outlet temperature decrease simultaneously, and temperature uniformity improves. Although the pressure drop and friction coefficient rise, the improvement in heat transfer performance outweighs these increases, resulting in a continuous increase in the comprehensive performance evaluation factor (PEC).

(2) The grooved structure enhances heat transfer by disrupting the thermal boundary layer on the wall surface and inducing vortices and secondary flow. Increasing the number of grooves can effectively reduce the peak temperature of the heat source, increase the Nusselt number, and improve temperature uniformity; however, it also increases flow resistance. Under the operating conditions of this study, a groove count of 8 achieves an optimal balance among heat transfer, temperature uniformity, and flow resistance; the marginal benefit of adding more grooves decreases significantly thereafter.

(3) The groove spacing has a significant impact on the heat transfer and flow characteristics of microchannels. The maximum heat source temperature, Nusselt number, and overall performance all follow a pattern of initially increasing and then decreasing. Excessively small spacing can easily lead to flow blockage and localized hot spots, while excessively large spacing allows the boundary layer to develop fully, resulting in weakened heat transfer. Under the operating conditions of this study, 3 mm is the optimal groove spacing, at which point the vortex structure develops fully, thermal resistance is minimized, and overall performance is optimal.

(4) The grooved microchannel structure outperforms the smooth microchannel in thermal-hydraulic performance across all investigated structural and operating conditions, verifying that passive flow disturbance via groove fabrication is an effective method to enhance heat dissipation of microchannel heat sinks for high-heat-flux electronic cooling applications.

This simulation result provides a theoretical basis for the optimized design of microchannel heat dissipation structures. Subsequent adjustments to the number of grooves can balance heat dissipation performance and pressure drop without compromising the circulation of the working fluid. That enables precise control of the heat source temperature and prevents increased system energy consumption due to excessive pressure drop.

Acknowledgement: Not applicable.

Funding Statement: The research findings in this paper were supported by the following funding projects, for which we express our sincere gratitude: Natural Science Foundation of Xinjiang Uygur Autonomous Region, China: Investigation on Thermal Performance of Microchannels with Enhanced Heat Transfer under High Heat Flux Conditions (Grant No. 2023D01C223); 2025 College Students' Innovation and Entrepreneurship Training Program Project: Experimental and Numerical Study on Gas-Liquid Two-Phase Transport Characteristics in Inclined Microchannels (Grant No. S202510997001); 2023 Changji University Research Grant: Stability Investigation of Phase-Change Microcapsules—A Pilot Experimental Study (Grant No. KYLK014).

Author Contributions: Hongxin Zhang: writing—review & editing, writing—original draft, methodology, investigation. Yi Zhang: software, writing—review & editing, data curation. Jiyun Tang: review & editing, supervision. Lei Yao: writing—review & editing, investigation. All authors reviewed and approved the final version of the manuscript.

Availability of Data and Materials: Data will be made available on reasonable request.

Ethics Approval: Not applicable.

Conflicts of Interest: The authors declare no conflicts of interest.

References

1. Yin Y, Zhu Y, Zhang D, Li Y, Gong L. A comprehensive analysis of flow and heat transfer performance in a novel Tesla valve microchannel. Case Stud Therm Eng. 2026;78:107670. [CrossRef].
2. Zhang X, Ji Z, Wang J, Lv X. Research progress on structural optimization design of microchannel heat sinks applied to electronic devices. Appl Therm Eng. 2023;235:121294. [CrossRef].
3. Hu C, Yang X, Wei J. Multilevel synergistic enhanced trapezoidal open microchannel heat sink for thermal management of electronic devices. Chin J Chem Eng. 2026;92:104–14. [CrossRef].
4. Kang Y, Luo ZB, Deng X, Zhu YX, Xia ZX, Cheng P. Research progress on microchannel enhanced heat transfer technology: Passive methods. Renew Sustain Energy Rev. 2025;224:116089. [CrossRef].
5. Al Kez D, Foley AM, Hasan Wong FWBM, Dolfi A, Srinivasan G. AI-driven cooling technologies for high-performance data centres: State-of-the-art review and future directions. Sustain Energy Technol Assess. 2025;82:104511. [CrossRef].
6. Nandan R, Arumuru V, Das MK. Prospects of hybrid cooling technologies for thermal management of electronic gadgets: A review. Int J Heat Mass Transf. 2026;255:127766. [CrossRef].
7. Pu X, Zhao Z, Sun M, Huang Y. Numerical study on temperature distribution uniformity and cooling performance of manifold microchannel heat sink. Appl Therm Eng. 2024;237:121779. [CrossRef].
8. Song Y, Fu R, Chen C, Wang Q, Su M, Hou F, et al. Case-embedded cooling for high heat flux microwave multi-chip array. Appl Therm Eng. 2022;214:118852. [CrossRef].
9. Gao J, Hu Z, Yang Q, Liang X, Wu H. Fluid flow and heat transfer in microchannel heat sinks: Modelling review and recent progress. Therm Sci Eng Prog. 2022;29:101203. [CrossRef].
10. Dong G, Huang C, Wu D, Liu S, Wu N, Huang P, et al. A review of the impacts of the microchannel structure on the heat transfer performance of microchannel heat exchangers. Int Commun Heat Mass Transf. 2025;169:109806. [CrossRef].
11. Tuckerman DB, Pease RFW. High-performance heat sinking for VLSI. IEEE Electron Device Lett. 1981;2(5):126–9. [CrossRef].
12. Zhu Q, Xia H, Chen J, Zhang X, Chang K, Zhang H, et al. Fluid flow and heat transfer characteristics of microchannel heat sinks with different groove shapes. Int J Therm Sci. 2021;161:106721. [CrossRef].
13. Kumar P. Numerical investigation of fluid flow and heat transfer in trapezoidal microchannel with groove structure. Int J Therm Sci. 2019;136:33–43. [CrossRef].
14. Liu X, Zhang H, Zhu C, Wang F, Li Z. Effects of structural parameters on fluid flow and heat transfer in a serpentine microchannel with fan-shaped reentrant cavities. Appl Therm Eng. 2019;151:406–16. [CrossRef].
15. Lv Q, Yan T, Feng Y, Huang H, Qin J. Experimental and numerical study of flow boiling heat transfer characteristics in rectangular groove-wall microchannels. Int J Heat Mass Transf. 2024;220:124999. [CrossRef].
16. Wang Q, Tao J, Cui Z, Zhang T, Chen G. Numerical simulation of fluid and heat transfer characteristics of microchannel heat sink with fan-shaped grooves and triangular truncated ribs. Int Commun Heat Mass Transf. 2024;155:107580. [CrossRef].
17. Wang Y, Liu J, Yang K, Liu J, Wu X. Performance and parameter optimization design of microchannel heat sink with different cavity and rib combinations. Case Stud Therm Eng. 2024;53:103843. [CrossRef].
18. Kuo CJ, Peles Y. Local measurement of flow boiling in structured surface microchannels. Int J Heat Mass Transf. 2007;50(23–24):4513–26. [CrossRef].
19. Sitar A, Sedmak I, Golobic I. Boiling of water and FC-72 in microchannels enhanced with novel features. Int J Heat Mass Transf. 2012;55(23–24):6446–57. [CrossRef].
20. Xia G, Chai L, Wang H, Zhou M, Cui Z. Optimum thermal design of microchannel heat sink with triangular reentrant cavities. Appl Therm Eng. 2011;31(6–7):1208–19. [CrossRef].
21. Hou T, Chen Y. Pressure drop and heat transfer performance of microchannel heat exchanger with different reentrant cavities. Chem Eng Process Process Intensif. 2020;153:107931. [CrossRef].
22. Liu L, Cao Z, Xu C, Zhang L, Sun T. Investigation of fluid flow and heat transfer characteristics in a microchannel heat sink with double-layered staggered cavities. Int J Heat Mass Transf. 2022;187:122535. [CrossRef].

23. Dong W, Zhang X, Liu B, Wang B, Fang Y. Research progress on passive enhanced heat transfer technology in microchannel heat sink. Int J Heat Mass Transf. 2024;220:125001. [CrossRef].
24. Gao W, Zhang JF, Qu ZG, Tao WQ. Numerical investigations of heat transfer in hybrid microchannel heat sink with multi-jet impinging and trapezoidal fins. Int J Therm Sci. 2021;164:106902. [CrossRef].
25. Hou T, Xu H, Jin F, Lin Y, Lin W. Heat transfer performance of microchannels with elliptic cavities based on field synergy principle and entropy production analysis. Int Commun Heat Mass Transf. 2025;166:109174. [CrossRef].
26. Saleh ZM, Al-Haidari SR. Numerical investigation of the effect of central inlet–dual outlet arrangement and sidewall fin shapes on the thermal-hydraulic performance of multi-channels cold plate. Int Commun Heat Mass Transf. 2026;173:110835. [CrossRef].
27. Hou T, Xu D. Pressure drop and heat transfer performance of microchannel heat exchangers with elliptical concave cavities. Appl Therm Eng. 2023;218:119351. [CrossRef].
28. Yang Z, Wang Y, Yuan X, Ding X, Yang G, Yang X, et al. Staggered counterflow rectangular microchannel liquid-cooled plate based on nanofluids for enhanced heat transfer performance. Int J Therm Sci. 2026;223:110651. [CrossRef].